Article

Cell Chemical Biology

MRSA Isolates from United States Hospitals Carry *dfrG* and *dfrK* Resistance Genes and Succumb to Propargyl-Linked Antifolates

Graphical Abstract

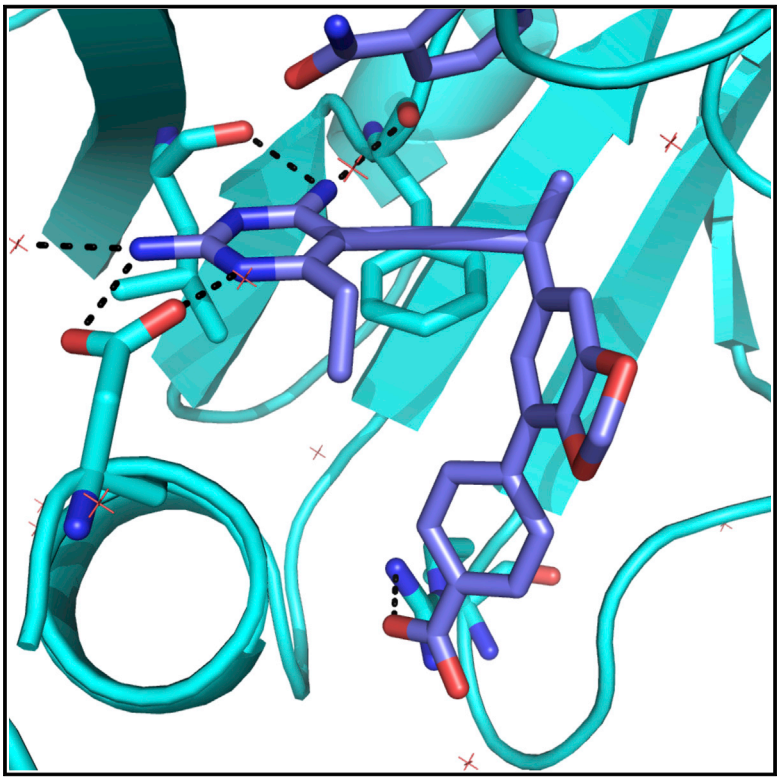

Highlights

- Three trimethoprim resistance genes have been identified in US MRSA isolates
- *dfrG and dfrK* are identified for the first time in US hospitals
- Propargyl-linked antifolates inhibit resistant enzymes and bacteria
- Structural studies indicate conserved arginine is responsible for potent activity

Authors

Stephanie M. Reeve, Eric W. Scocchera, Narendran G-Dayanadan, ..., Jeffrey Aeschlimann, Dennis L. Wright, Amy C. Anderson

Correspondence

dennis.wright@uconn.edu

In Brief

Reeve et al. identified two plasmid-borne genes that confer high-level resistance to trimethoprim for the first time in MRSA isolates from US hospitals. A series of charged propargyl-linked antifolates overcome this resistance via direct inhibition of the acquired resistance elements.

Reeve et al., 2016, Cell Chemical Biology *23*, 1–10
December 22, 2016
http://dx.doi.org/10.1016/j.chembiol.2016.11.007

CellPress

Please cite this article in press as: Reeve et al., MRSA Isolates from United States Hospitals Carry *dfrG* and *dfrK* Resistance Genes and Succumb to Propargyl-Linked Antifolates, Cell Chemical Biology (2016), http://dx.doi.org/10.1016/j.chembiol.2016.11.007

Cell Chemical Biology
Article

MRSA Isolates from United States Hospitals Carry *dfrG* and *dfrK* Resistance Genes and Succumb to Propargyl-Linked Antifolates

Stephanie M. Reeve,[1] Eric W. Scocchera,[1] Narendran G-Dayanadan,[1] Santosh Keshipeddy,[1] Jolanta Krucinska,[1] Behnoush Hajian,[1] Jacob Ferreira,[1] Michael Nailor,[2,3] Jeffrey Aeschlimann,[2,4] Dennis L. Wright,[1,5,*] and Amy C. Anderson[1]
[1]Department of Pharmaceutical Sciences
[2]Department of Pharmacy Practice
University of Connecticut, 69 North Eagleville Road, Storrs, CT 06269, USA
[3]Department of Pharmacy Services, Hartford Hospital, 80 Seymour Street, Hartford, CT 06102, USA
[4]Division of Infectious Diseases and Department of Pharmacy Services, UConn Health/John Dempsey Hospital, 263 Farmington Avenue, Farmington, CT 06030, USA
[5]Lead Contact
*Correspondence: dennis.wright@uconn.edu
http://dx.doi.org/10.1016/j.chembiol.2016.11.007

SUMMARY

Antibiotic resistance is a rapidly evolving health concern that requires a sustained effort to understand mechanisms of resistance and to develop new agents that overcome those mechanisms. The dihydrofolate reductase (DHFR) inhibitor, trimethoprim (TMP), remains one of the most important orally administered antibiotics. However, resistance through chromosomal mutations and mobile, plasmid-encoded insensitive DHFRs threatens the continued use of this agent. We are pursuing the development of new propargyl-linked antifolate (PLA) DHFR inhibitors designed to evade these mechanisms. While analyzing contemporary TMP-resistant clinical isolates of methicillin-resistant and sensitive *Staphylococcus aureus*, we discovered two mobile resistance elements, *dfrG* and *dfrK*. This is the first identification of these resistance mechanisms in the United States. These resistant organisms were isolated from a variety of infection sites, show clonal diversity, and each contain distinct resistance genotypes for common antibiotics. Several PLAs showed significant activity against these resistant strains by direct inhibition of the TMP resistance elements.

INTRODUCTION

Methicillin-resistant *Staphylococcus aureus* (MRSA) continues to spread globally causing moderate to life-threatening infections. The organism can be acquired through nosocomial (HA-MRSA) or community (CA-MRSA) routes; CA-MRSA and HA-MRSA are genetically distinct and have differing patterns of antibiotic resistance; however CA-MRSA is now epidemic within health care systems (Lodise and McKinnon, 2007; Bush et al., 2015). Trimethoprim-sulfamethoxazole (TMP-SMX), branded as Bactrim and Septra, is a first-line treatment for MRSA infections in the community setting (Frei et al., 2010; Gorwitz et al., 2006; Nathwani et al., 2008; Liu et al., 2011), owing to its oral bioavailability, low cost, and general tolerability. In fact, prescriptions of TMP-SMX numbered more than 21 million in 2013, putting it in the group of top ten oral antibiotics prescribed in 2013 (Centers for Disease Control and Prevention, 2013). This combination therapy employs two drugs that synergistically inhibit the folate biosynthetic pathway, which is essential for the production of deoxythymidine monophosphate, purine nucleotides, and some amino acids. Trimethoprim (TMP) is an inhibitor of dihydrofolate reductase (DHFR) and SMX inhibits dihydropteroate synthase.

Resistance to TMP-SMX in *S. aureus* began to arise in the 1980s (Dale et al., 1995, 1997; Huovinen et al., 1995). Reports of contemporary TMP-SMX resistance vary regionally: 21% of resistance is reported in travel clinics in Europe (Nurjadi et al., 2015), whereas ~3% has been reported in a group of US hospitals (Sader et al., 2015). TMP-SMX resistance is on the rise according to a survey of 2,193 isolates showing that TMP-SMX resistance rose from 3.4% in 2007 to 6% in 2012 (Pate et al., 2014). The mechanisms of resistance are temporally segregated. In the 1990s, point mutations were observed in the chromosomal gene, *dfrB* in *S. aureus*; these modifications of the enzyme were responsible for increases in minimum inhibitory concentration (MIC) values to 256 μg/mL (~800-fold). Noteworthy in this group was the F98Y mutation that conferred ~400-fold decrease in affinity between TMP and DHFR (Dale et al., 1997). Compensatory double mutations (F98Y/H149R and F98Y/H30N) arose that increased the fitness of the mutated enzyme. Horizontally transferred, plasmid-encoded resistant DHFR enzymes also appeared. The translated protein of the *dfrA* gene, often called S1 (but called DfrA here for clarity), was observed to confer 338-fold resistance to TMP at the enzyme level (Dale et al., 1995). DfrA has three mutations in comparison with DHFR from the TMP-sensitive *S. epidermidis*: V31I, G43A, and F98Y; F98Y is the major determinant of loss of affinity. The resistance gene, *dfrG*, was first reported in isolates from Thailand (Sekiguchi et al., 2005) and was later reported as abundant in sub-Saharan Africa (Nurjadi et al., 2014) with subsequent isolation

Table 1. Characterization of TMP^R Clinical Isolates

Strain Designation	Infection Source	TMP-Resistant Gene	*dfrB*	TMP MIC (μg/mL)	SMX MIC (μg/mL)	Doubling Time (min)
UCH MRSA 1	blood	*dfrG*	WT	>1,000	>500	40.33
UCH MRSA 115	SSTI	*dfrA*	WT	250	500	35.19
UCH MRSA 121	sputum	*dfrG*	WT	>1,000	>500	28.17
UCH MRSA 127	SSTI	*dfrG*	WT	>1,000	16	38.61
HH MRSA 714	SSTI	*dfrG*	WT	>1,000	>500	27.39
HH MRSA 1144	SSTI	*dfrA*	WT	250	>500	32.54
HH MRSA 1184	sputum	*dfrK*	WT	>1,000	32	29.38
UCH MSSA 1	sinus cavity	*dfrG*	WT	>1,000	>500	36.49
Sa43300	ATCC	none	WT	0.3125	8	38.16

SSTI, skin and soft tissue.

from European travelers who had visited Africa. This later study reported that 54% of 598 isolates were resistant to TMP and 19% to the combination of TMP-SMX. The gene *dfrK* was originally identified in swine in multi-drug-resistant MRSA ST398 where it caused MIC values to rise to 256 μg/mL (Kadlec and Schwarz, 2010), but began to be observed in farmers with MRSA infections. In 2012, an MRSA isolate from a patient in Spain was identified as linezolid-resistant, carrying the ERGB plasmid that links resistance genes *cfr* (oxazolidinones, phenicols, lincosamides, pleuromutilins, and streptogramin A), *ant(4′)-Ia* (tobramycin), *tet*(L) (tetracycline), and *dfrK* (TMP) (de Gopegui et al., 2012). DfrG and DfrK, like DfrA, are innately resistant enzymes carried on plasmids and incorporated into the chromosome via horizontal gene transfer. DfrG and DfrK share 89% sequence similarity to each other, however, they are less similar to DfrA (38% and 39%) and DfrB (41% and 42%). The origins of DfrG and DfrK are unknown. No recent survey of MRSA isolates from US hospitals has identified common molecular mechanisms of TMP-SMX resistance.

Over the past decade, we have focused on the development of next generation propargyl-linked antifolates (PLAs) that maintain activity against many of the important pathogenic bacterial DHFR enzymes while expanding coverage to include both mutant and naturally TMP-insensitive DHFR enzymes that give rise to TMP resistance within *S. aureus* (Frey et al., 2009, 2010a, 2012; Keshipeddy et al., 2015; Lamb et al., 2014; Lombardo et al., 2016). The occurrence of a common F98Y mutation shared by resistant *S. aureus* mutants and plasmid-encoded DHFRs provided rationale that new antifolates that are effective against this mutant could expand coverage for these resistant enzymes. We anticipated that optimizing the PLAs to overcome the central F98Y resistance mechanism would lead to robust inhibitors capable of targeting multiple enzymes that possess this substitution. Recently we reported a series of PLAs that potently inhibit the F98Y mutant enzyme as well as *S. aureus* strains harboring the F98Y mutation (Keshipeddy et al., 2015).

As antibiotic resistance is a naturally evolving phenomenon, it is critical to map compound design to contemporary resistance profiles found in clinical strains of bacteria to properly target the prevailing molecular mechanisms during lead optimization. In the work described here, we present a recent investigation of the molecular mechanisms of TMP resistance for MRSA and methicillin-sensitive *Staphylococcus aureus* (MSSA) isolated in the state of Connecticut, the results of which have guided compound development to yield potent inhibitors of an emerging group of TMP-resistant strains. We collected clinical isolates of TMP-resistant MRSA over a 2-year period to determine which mechanisms are currently predominant. Using whole-genome sequencing and PCR, we identified the plasmid-encoded *dfrG, dfrA*, and *dfrK* genes in these isolates. It is noteworthy that this is the first report of the resistance-conferring *dfrG* and *dfrK* genes in strains of MRSA and MSSA in the United States. Interestingly, we did not identify any of the well-characterized mutations to the chromosomal gene, *dfrB*. Excitingly, several of the PLAs potently inhibit the growth of the clinical isolates that possess these plasmid-encoded *dfrA*, *dfrG*, and *dfrK* genes as well as inhibit the purified enzymes at nanomolar levels of potency.

RESULTS

Clinical Bacterial Isolates of MRSA and MSSA Harbor dfrA, dfrG, and dfrK

Over the past 2 years, we obtained several TMP-resistant strains from the clinical microbiology laboratories at UConn Health/John Dempsey Hospital (UCH) and Hartford Hospital (HH) isolated in the course of routine clinical care. The strains were originally submitted for routine susceptibility testing. TMP-SMX resistance rates at UCH and HH are reported at ≤1% and 2% for MSSA and 2%–3% and 5% for MRSA isolates, respectively. Seven of the obtained strains were classified as MRSA and one was MSSA. These strains were collected from different patients and from a variety of sources including blood, skin and soft tissue, sputum, and the sinus cavity. The blood sample was derived from a hospitalized patient; the other isolates were derived from outpatients. Clearly, each of the strains is highly resistant to TMP and SMX, with MIC values between 250 and >1,000 μg/mL or 16–500 μg/mL, respectively (Table 1). The strains show varying resistance profiles to a wide range of commonly used antibiotics including erythromycin, fluoroquinolones, aminoglycosides, and tetracycline (Table S1).

To determine the molecular basis of TMP resistance, we initially probed for mutations in the chromosomal *dfrB* gene. Somewhat surprisingly, no mutations were observed in any of the strains. To investigate further, we initially conducted whole-genome sequencing on a single strain, UCH MRSA 1. Genomic

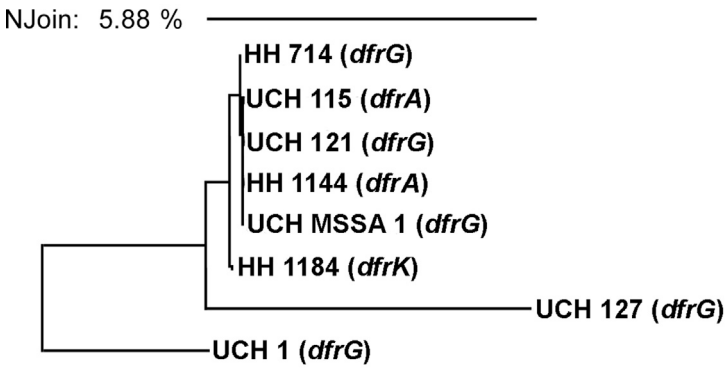

Figure 1. Clonal Characterization of *S. aureus* Strains by *spaA* Sequencing

analysis revealed the presence of a second DHFR enzyme encoded by the gene, *dfrG*, that had been integrated into the chromosome. Although this gene has been observed in *S. aureus* in Asian (Sekiguchi et al., 2005), African, and European travelers (Nurjadi et al., 2014), and in *Streptococcus pyogenes* in India (Bergmann et al., 2014), to our knowledge, this is the first report of *dfrG* in North America. We then used PCR to evaluate the remaining strains for the presence of *dfrG* as well as two other plasmid-encoded genes, *dfrA* and *dfrK*, known to occur in *S. aureus*. Surprisingly, we found that all of the clinical isolates carried one of the plasmid-encoded genes, with the *dfrG* gene predominating (Table 1). We also identified, for the first time in the United States, the presence of the *dfrK* gene. The better characterized *dfrA* appeared in the remaining two strains (Table 1, Figure S1). One report (de Gopegui et al., 2012) showed that the presence of *dfrK* was associated with *cfr*, a gene that confers linezolid non-susceptibility. We probed the strains for the *cfr* gene, but no strains, even HH1184 that contains *dfrK*, positively identified the gene. This result correlates with the observed linezolid susceptibility of all of the strains (Table S1). Interestingly, the acquisition of these *dfr* genes did not appear to be associated with obvious negative fitness costs as the doubling times were generally shorter than the ATCC 43300 strain (Table 1).

Given the limited number of strains presented here, the occurrence of these diverse resistance elements is striking. To better understand the possible relationships of these TMP-resistant strains, the genetic diversity was determined through sequencing of the *spaA* gene (Petersson et al., 2010). The analysis showed that five of the strains (UCH MRSA 115, UCH MRSA 121, UCH MSSA 1, HH MRSA 714, and HH MRSA 1144), including strains from both hospitals and the MSSA strain, were clonally indistinguishable. However, UCH MRSA 127, HH MRSA 1184, and UCH MRSA 1 are clonally distinct isolates. Importantly, within the group of five clonal isolates, *dfrA* and *dfrG* are represented and *dfrK* is found to be a distinct yet related strain, HH MRSA 1184, Figure 1. The appearance of the different *dfr* isoforms within the closely related cluster as well as more genetically distinct strains suggests that they are on potentially highly mobile resistance elements.

Clinical Isolates Exhibit a Range of Antibiotic Susceptibilities

The phenotypes to commonly prescribed non-TMP antibiotics were determined for the isolates revealing diverse variability in susceptibilities. All strains were susceptible to vancomycin, linezolid, rifampin, and daptomycin and have varied susceptibilities to SMX, erythromycin, clindamycin, tetracycline, gentamicin, and a variety of fluoroquinolones, based on breakpoint MICs (Table S1). To better understand the diversity of the isolates, the remaining seven genomes were sequenced and the molecular mechanisms of resistances were identified. Interestingly, the only common resistance mechanism found within the clonal group of strains was five previously reported *folP* mutations (F17L, T28S, T59S, L64M, and E205K) conferring high-level SMX resistance. UCH1 contains 13 *folP* mutations (F17L, V30I, T31N, M37I, I58V, T59S, V60L, L64M, I110M, V117I, V126I, E208K, and F226L) while HH1184 contains 9 (V30I, I58V, T59S, V60L, L64M, I100M, V117I, V126I, and F226L) increasing the MIC to near its clinical resistance breakpoint (Hampele et al., 1997). TetM, a ribosome protection protein, is identified as the tetracycline-resistance determinant observed in UCH115 and HH1144 (Trzcinski et al., 2000). Gentamicin resistance in UCH115 and HH1144 is conferred by a plasmid-borne AAC(6′)-APH(2″) aminoglycoside-resistance enzyme (Daigle et al., 1999). Tetracycline and aminoglycoside resistance was only identified in strains containing *dfrA*; however, these strains differ both in fluoroquinolone-resistance mechanisms and macrolide susceptibility.

Resistance to fluoroquinolone in all strains except HH MRSA 1184 is conferred through a variety of mutations in the quinolone-resistance-determining regions of DNA gyrase subunit A (*gyrA*) and topoisomerase IV, subunits A and B (*grlA* and *grlB*). Combinations of mutations varying from single *gyrA* mutations to the accumulation of four mutations between *gyrA*, *grlA*, and *grlB* were observed (Schmitz et al., 1998; Pan et al., 2002). NorA efflux activity in fluoroquinolone resistance was determined by MIC in the presence of reserpine, a NorA inhibitor. Minimal shifts in MIC for levofloxacin and up to 8-fold decrease in ciprofloxacin MIC indicate that NorA has minimal influence on fluoroquinolone resistance (Table S3) (Kaatz and Seo, 1995; Aeschlimann et al., 1999). *mphC*, a 2'-phosphotransferase which directly inactivates the macrolides via phosphorylation determines selective macrolide resistance (erythromycin) in UCH121, UCH127, and HH1184, all clonally distinct isolates (Matsuoka et al., 2003; Juda et al., 2016). *mphC* is not commonly reported to confer macrolide resistance in human *S. aureus* isolates, instead it is more frequently reported in agricultural studies (Li et al., 2015). *ermC*, a 23s rRNA methyl transferase, found in

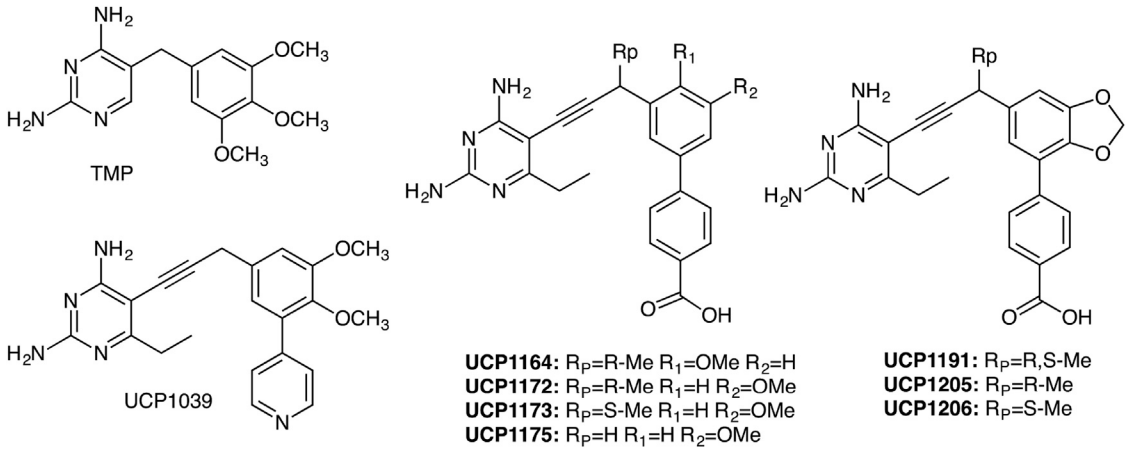

Figure 2. Structure of PLAs in This Study

UCH MRSA 1, HH MRSA 1144, and UCH MSSA 1 confers resistance to both macrolides and lincosamines (clindamycin) (Khan et al., 1999). HH MRSA 1184 is the only strain to contain the Panton-Valentine leukocidin, a virulence factor that produces a cytotoxin associated with tissue necrosis and leukocyte damage (Lina et al., 1999). All strains clinically classified as "methicillin resistant" via susceptibility are *mecA* positive. A full list of target mutations, efflux activity, and resistance determinants are summarized in Tables S2 and S3.

PLAs Potently Inhibit Clinical Isolates

Whole-genome sequencing of the clinical strains showed notable variation in the molecular basis of TMP resistance as well as several common antibiotics. This provided a useful panel of clinically relevant strains as an important tool for lead optimization. Therefore, we screened a variety of previously developed PLA lead compounds against the panel of TMP-resistant strains to identify candidates with broad activity. Excitingly, several of the compounds (UCP1039, UCP1164, UCP1172, UCP1173, and UCP1175; Figure 2, Tables 2 and 3) showed very potent activity against these highly TMP-resistant strains. Although we observed activity with earlier-generation inhibitors that contained a pyridyl C-ring (e.g., UCP1039, Figure 2 and Table 2), the most potent activity was observed with a recently disclosed charged/zwitterionic series possessing an ionizable carboxylic acid on the distal C-ring (UCP1164, UCP1172, UCP1173, and UCP1175). Overall, the PLAs were most potent against strains carrying *dfrG* and *dfrK* with MIC values as low as 0.1563 μg/mL, 2-fold lower than the MIC for TMP against wild-type *S. aureus*. Compound UCP1173 showed the most potent activity against strains possessing *dfrA* with MIC values of 1.25 and 2.5 μg/mL. Interestingly, compound UCP1172 is the antipodal point of UCP1173 but does not significantly inhibit *dfrA*-possessing strains.

It was noted that C3′, C4′ dioxygenation with a pyridyl C-ring (UCP1039) afforded some of the strongest activity in this series and, as such, we investigated the combination of this pattern of functionality with the preference for a C-ring carboxylic acid. To explore this design, a dioxalane ring was chosen as a convenient isostere as it afforded antibacterial activity against strains that possessed a DHFR with the F98Y mutation (Keshipeddy et al., 2015). Using routes described previously (Keshipeddy et al., 2015), we synthesized racemic inhibitor UCP1191 and the individual enantiomers, UCP1205 and UCP1206. We were delighted to see a significant increase in activity against both *dfrG*- and *dfrK*-possessing strains with MIC values of 0.1563–0.625 μg/mL. Interestingly, despite these strains also being SMX resistant, an apparently strong synergistic interaction between the PLAs and SMX was observed (Tables 2 and S4).

Further validation that the antibacterial activity of the PLAs in these resistant organisms was directly related to their ability to inhibit the resistance-conferring enzymes was provided by cloning, expressing, purifying, and evaluating enzyme inhibition. The three genes, *dfrA*, *dfrG*, and *dfrK* were cloned into expression vectors and the resulting proteins purified to homogeneity. The PLAs were evaluated for enzyme inhibition using standard assays that measure the oxidation of the NAPDH co-factor (Table 3) (Frey et al., 2009, 2010a, 2010b, 2012; Keshipeddy et al., 2015; Reeve et al., 2014, 2016). As expected, TMP exhibits high inhibition concentration 50% (IC_{50}) values for all three TMP-resistant DHFRs. Despite the fact that there has been no directed optimization of the PLAs against these TMP-resistant proteins, the PLAs showed relatively potent inhibition with the majority of IC_{50} values less than 100 nM, highlighting the value of our approach to use structure-based targeting of common resistance mechanisms in DHFRs (Keshipeddy et al., 2015; Reeve et al., 2016). Remarkably, this is an approximately 4,400-, 55-, or 2,000-fold increase in potency over TMP for the DfrG, DfrA, and DfrK proteins, respectively. Although a variety of factors beyond target inhibition contribute to the overall antibacterial activity, there is a correlation between PLA activity against the TMP-resistant enzymes and the MICs against the corresponding strains. Additional validation that the PLAs exert their antibiotic effect through blockade of the folate pathway was provided by rescue experiments whereby the culture medium was supplemented with thymidine, and MIC values rose by at least 8-fold (data not shown). The potent inhibitors described above, specifically those with zwitterionic character, are promising drug leads that show strong antibiotic activity, low mammalian cell toxicity, and good metabolic stability (Scocchera et al., 2016).

Table 2. PLA Antibacterial Activity against Clinical Isolates

	MIC Values (μg/mL)								
Inhibitor	UCH MRSA 1 (*dfrG*)	UCH MRSA 115 (*dfrA*)	UCH MRSA 121 (*dfrG*)	UCH MRSA 127 (*dfrG*)	HH MRSA 714 (*dfrG*)	HH MRSA 1144 (*dfrA*)	HH MRSA 1184 (*dfrK*)	UCH MSSA 1 (*dfrG*)	ATCC 43300
UCP1039	1.25	>20	0.625	0.3125	1.25	>10	1.25	0.625	0.0391
UCP1164	2.5	10	5	2.5	5	5	0.625	5	0.0391
UCP1172	0.625	5	0.625	0.3125	0.625	5	0.3125	0.3125	0.0098
UCP1173	5	2.5	5	2.5	5	1.25	2.5	2.5	0.0098
UCP1175	2.5	>20	10	5	10	>20	5	10	0.0195
UCP1191	0.625	20	0.625	0.1563	0.625	10	0.1563	0.3125	0.0195
UCP1205	0.625	>10	0.625	0.3125	0.625	>10	0.3125	0.3125	0.0195
UCP1206	2.5	>10	2.5	1.25	2.5	>10	1.25	1.25	0.0098
UCP1191 + SMX[a]	0.0391	00.625	0.0781	0.3125	0.0391	0.625	≤0.0098	0.0098	≤0.0048

[a]MIC values with 100 μg/mL sulfamethoxazole (SMX), ATCC 43300, and UCH127 at 1 μg/mL SMX.

Crystal Structure of *S. aureus* DHFR with UCP1191

A high-resolution (1.88 Å) crystal structure of wild-type SaDHFR bound to compound UCP1191 (diffraction data and model statistics are shown in Table S5, omit map shown in Figure S2, and structural analysis of interactions are shown in Table S5) reveals a potential basis for the increased potency of this series of PLA-COOH compounds with both the wild-type and TMP-resistant enzymes. The diaminopyrimidine of the antifolate forms conserved hydrogen bonds with Asp27 and backbone carbonyl oxygen atoms from Leu5 and Phe92 (Figure 3). The propargyl linker and benzodioxalane B-ring form hydrophobic interactions with Phe92, Thr46, Leu28, Val31, and Ile50. The phenyl C-ring is positioned well to form hydrophobic interactions with Leu54, Val31, and Leu28. Importantly, the carboxylate moiety forms one direct ionic bond to Arg57 and one water-mediated hydrogen bond to Arg57 and Lys32. In earlier versions of the PLA-COOH compounds that possess a phenyl B-ring (similar to, e.g., UCP1164) the carboxylate forms an extensive water network with Arg57 (Reeve et al., 2016) as opposed to this more direct interaction between UCP1191 and Arg57. Arg57 is conserved in all of the TMP-resistant enzymes (Figure 3) and forms a similar key contact with dihydrofolate (Scocchera et al., 2016), suggesting that this contact is less likely to mutate to cause resistance to the PLAs.

Interestingly, the TMP-resistant enzymes tend to conserve their mechanisms of reducing TMP affinity (Figure 4). Leu5 is an isoleucine in the TMP-resistant enzymes; this mutation would disturb Phe92, which is critical both for hydrogen bonding (through the backbone carbonyl to the 4-amino group of the pyrimidine) as well as hydrophobic interactions with the linker. Leu28 is a tyrosine in DfrG and DfrK, and Val31 is Ile in DfrA; these mutations also perturb Phe92. The Val31 Ile mutation was predicted by K* in the OSPREY suite to cause resistance to an earlier PLA, and in fact reduced affinity by 60-fold (Frey et al., 2010b; Reeve et al., 2014). Crystal structures of the double-mutant enzyme, F98Y/V31I, show the perturbation of Phe92. His30 mutations have been observed clinically in the *dfrB* gene (Dale et al., 1997). While the mutation His30Asn has been shown to disrupt the water network stabilizing the pyrimidine ring (Frey et al., 2010a; Reeve et al., 2016), the TMP-resistant enzymes DfrK and DfrG carry a tyrosine at this position, which may achieve the same goal. Finally, all three TMP-resistant enzymes maintain a tyrosine at position 98 (WT Phe). The tyrosine has been shown to perturb NADPH binding (Frey et al., 2009; Keshipeddy et al., 2015) and to decrease synergistic binding between TMP and NADPH (Heaslet et al., 2009).

Previous design efforts focused on achieving inhibitor potency against the mutations observed in the chromosomal copy, *dfrB*, such as the Phe98Tyr-mutated DHFR enzyme (Keshipeddy et al., 2015; Reeve et al., 2016; Oefner et al., 2009a, 2009b; Heaslet et al., 2009).

These efforts may prove valuable as the TMP-resistant enzymes DfrG, DfrK, and DfrA all possess a tyrosine residue at position 98. As shown here, designing inhibitors against the F98Y chromosomal mutant provided a significant advantage in achieving superior potency against these resistant enzymes, as they appear to rely on common mechanisms. Recently, we described potent activity of the COOH-PLA series, specifically UCP1164, UCP1172, UCP1173, and UCP1175 against strains containing these clinically relevant point mutations in *dfrB*. Including F98Y and F98Y with H30N and H149R. While the COOH-PLAs are more potent against the single F98Y mutant strain than the acquired *dfr* isoforms, UCP1164 and UCP1172 maintain superior activity against the acquired resistance elements over the double mutants. The remaining compounds display similar inhibitory activity in the acquired and mutant DHFR enzymes (Reeve et al., 2016). As the mutations that confer TMP resistance appear to belong to a conserved and relatively manageable group, future design efforts can capitalize on this group to optimize ligands that inhibit the majority of clinically observed TMP-resistant species.

DISCUSSION

TMP-SMX has been a mainstay for treating *S. aureus* infections in the community setting for decades. Despite knowledge of the existence of the plasmid-encoded resistance elements *dfrG* and *dfrK* since 2005, their importance in clinical strains of MRSA and MSSA in the United States was not thought to be significant and antifolate development was often targeted toward resistant

Table 3. Enzyme Inhibition

	IC_{50} Values (μM)			
Inhibitor	DfrB (wt SaDHFR)	DfrG	DfrA	DfrK
TMP	0.023 ± 0.002	380 ± 12	15.1 ± 0.7	43 ± 2
UCP1039	0.014 ± 0.001	0.45 ± 0.02	0.36 ± 0.02	0.022 ± 0.003
UCP1164	0.037 ± 0.002	1.4 ± 0.1	8.8 ± 0.9	0.073 ± 0.002
UCP1172	0.0089 ± 0.0007	0.22 ± 0.02	0.41 ± 0.01	0.030 ± 0.001
UCP1173	0.014 ± 0.001	0.19 ± 0.01	0.27 ± 0.02	0.091 ± 0.008
UCP1175	0.0110 ± 0.0006	1.4 ± 0.2	0.98 ± 0.008	0.17 ± 0.01
UCP1191	0.010 ± 0.0002	0.087 ± 0.005	0.32 ± 0.03	0.041 ± 0.006
UCP1205	0.018 ± 0.003	0.159 ± 0.007	0.34 ± 0.01	0.10 ± 0.01
UCP1206	0.017 ± 0.002	0.19 ± 0.01	0.18 ± 0.03	0.054 ± 0.005

mutants of the chromosomal gene. Herein, we show a surprising preponderance of these genes from a relatively small collection of TMP-resistant MRSA/MSSA isolates from two Connecticut hospitals. Genetic analysis of the strains supports that these elements are potentially easily transferred between bacteria, suggesting that occurrence of these genes may be much wider than reported. The report here of these new elements in the United States is highly concerning as they confer extremely high levels of resistance to TMP, appear to be very mobile and are associated with a wide range of infections.

Building a program to understand the structural mechanisms of TMP resistance has supported the design of PLAs that potently inhibit both TMP-resistant enzymes and the strains harboring these elements. Here, the identification of the *dfrG* and *dfrK* genes in clinical isolates has fostered the refinement of these inhibitors to arrive at highly potent antibacterial agents. Furthermore, the clinical relevancy of the compounds remains acute as timely clinical data drive compound design.

SIGNIFICANCE

The continued spread of antibiotic-resistance elements between pathogenic bacterial strains is diminishing the lifetime of many first-line antibiotics, leaving limited treatment options for bacterial infections. Only by investigating the contemporary mechanisms of antibacterial resistance is it possible to design new antibiotics that will efficaciously inhibit the resistant bacteria that are currently circulating in hospitals, assisted-care living, and the wider community. Here, we report the first identification of two plasmid-borne genes found in clinical *Staphylococcus aureus* isolates from United States hospitals as well as identify the molecular mechanisms of resistance to several common antibiotics. The clinical impact of these genes, *dfrG* and *dfrK*, is significant as the resulting proteins confer high levels of trimethoprim resistance and render this commonly used antibiotic useless. In addition, the fact that each of the strains presented here possesses plasmid-borne enzymes speaks to the potential widespread existence of these resistant strains. Using a structure-based approach designed to overcome trimethoprim-resistant enzymes, a series of charged propargyl-linked antifolates are presented that directly target the acquired resistance elements and potently inhibit the resistant enzymes and bacteria.

EXPERIMENTAL PROCEDURES

Clonal Analysis

SpaA-typing was performed by Charles River using Accugenix's AccuGENX-ST service to identify clonality among isolates.

Genomic Sequencing of Clinical Isolates

Genomic DNA was isolated using the Promega Wizard Genomic DNA Isolation Kit. DNA extracts were quantified using the Quant-iT PicoGreen Kit (Invitrogen, Thermo Fisher Scientific). One nanogram of genomic DNA was fragmented, adapter sequences attached, size selected, and cleaned using the Nextera XT Library Preparation Kit (Illumina) according to the manufacturer's protocol. Libraries were validated and mean insert length was calculated using a Bioanalyzer High Sensitivity chip (Agilent Technologies). The libraries were sequenced on the MiSeq using v2 2x250 base pair kit (Illumina). The genome was assembled using CLC Workbench and annotated using the RAST Server (Aziz et al., 2008; Brettin et al., 2015; Overbeek et al., 2014). The assembled and annotated genomes are available through the corresponding author.

PCR Identification and Sequencing

PCR on gel-purified genomic and plasmid DNA was performed to detect the presence of *dfrB*, *dfrA*, *dfrG*, and *dfrK* genes. PCR was performed using rTaq Polymerase (TaKaRa) and reactions were run on 1.2% agarose gels and visualized with ethidium bromide using 2-Log Ladder as a size comparator (Thermo Fisher Scientific). PCR product was purified using the Promega SV Gel and PCR Clean-Up System and sequenced using the corresponding sense primer to confirm the gene identity.

MICs

MICs for UCP compounds, TMP, SMX (Dao et al., 2014), levofloxacin, linezolid (in DMSO), erythromycin (in ethanol), and ciprofloxacin (in 0.1 N HCl) were determined following CSLI guidelines from methods described previously (Clinical and Laboratory Standards Institute, 2014).

Clinical Antibiotic Susceptibility

Susceptibilities were determined using Sensititre Gram Positive Plates (Remel, Thermo Fisher Scientific) using Mueller-Hinton Broth and an inoculum of 1×10^5 colony-forming unit/mL. The plates were incubated for 18 hr at 37°C and MICs were colorimetrically determined using alamarBlue (Thermo Fisher Scientific). Susceptible/intermediate/resistant designations were made based on CLSI breakpoint standards (Clinical and Laboratory Standards Institute, 2014).

DfrA, DfrB, DfrG, and DfrK Protein Expression and Purification

The expression and purification of *dfrB* in pET-41a(+) has been described previously (Frey et al., 2009, 2012; Reeve et al., 2016). BL21 (DE3) cells (Invitrogen) were transformed with DfrA and DfrG in pET-41a(+) and DfrK in pET-24-a(+). The cells were grown to mid-log phase at 37°C, induced with 1 mM isopropyl-thio-β-D-galactoside, and were allowed to grow for an additional 18 hr at

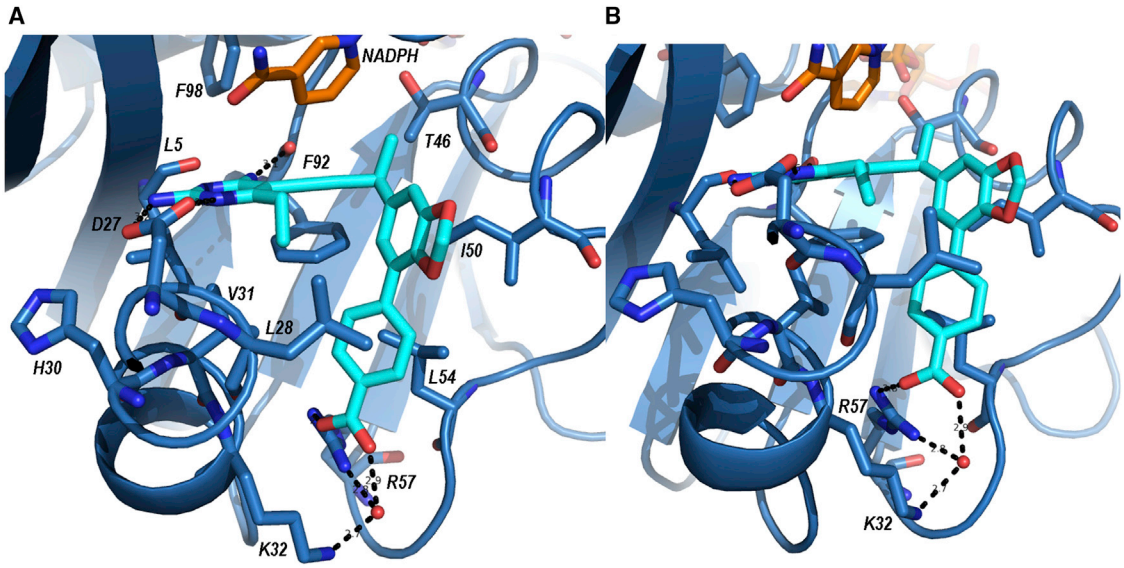

Figure 3. Crystal Structure of SaDHFR Bound to NADPH, Orange, and UCP1191, Cyan
An overview of the ligand in the active site (A); a more detailed view of the interaction with Arg 57 (B). The hydrogen bonding interactions between the protein and inhibitor are shown in black (PDB: 5JG0).

20°C. Cells were pelleted and resuspended to 30 mL using a buffer containing 0.4 M KCl, 25 mM Tris (pH 8.0), 5 mM β-mercaptoethanol, 5% glycerol, 100 μg/mL lysozyme, 5 mM imidazole, and DNase (Thermo Fisher Scientific) and lysed via sonication. DfrG was resuspended to 30 mL using a buffer containing 0.5 M KCl, 50 mM Tris (pH 8.0), 5 mM β-mercaptoethanol, 5% glycerol, 0.8 mg/mL lysozyme, 5 mM imidazole, DNase, RNase, and a protease inhibitor tablet (Life Technologies) and lysed via French Press.

Protein was purified using Ni-NTA agarose using a wash buffer containing 25 mM Tris (pH 8.0), 0.4 M KCl, 5 mM imidazole, 5 mM β-mercaptoethanol, and 5% glycerol, and protein was eluted using a buffer containing 25 mM Tris (pH 8.0), 0.3 M KCl, 20% glycerol, 0.1 mM EDTA, 250 mM imidazole, and 5 mM β-mercaptoethanol. Clean protein was pooled and desalted into a buffer containing 25 mM Tris (pH 8.0), 0.1 mM KCl, 15% glycerol (20% for DfrG), 0.1 mM EDTA, and 2 mM DTT. Protein was flash frozen and stored at −80°C.

IC_{50} Determination

IC_{50} values were determined following a standard method that has been described previously (Reeve et al., 2014, 2016).

DfrB:NADPH:UCP1191 Crystallography

Purified DfrB at 13 mg/mL protein was co-crystallized with 2 mM NADPH and 1 mM UCP1191 in DMSO via the hanging-drop method. The mixture of protein and co-factor was incubated on ice for 3 hr. Equal volumes of protein solution were added to an optimized buffer solution containing 0.1 M 2-(N-morpholino) ethanesulfonic acid (pH 5.0), 0.3 M sodium acetate, 17% PEG 10,000, and 12.5% γ-butyrolactone. When stored at 4°C, crystals typically formed within 7 days. Crystals were harvested and frozen in cryo-protectant buffer containing 25% glycerol. Data were collected remotely on beamline 14-1 at Stanford Synchrotron Radiation Lightsource, SLAC National Accelerator Laboratory. Data were indexed and scaled using HKL-2000. Phaser was used to identify molecular replacement solutions using PDB: 3F0Q (Frey et al., 2009) as a probe. Coot (Emsley and Cowtan, 2004) and Phenix (Adams et al., 2010) were used for structure refinement until acceptable R_{work} and R_{free} were achieved.

Doubling Time Determination

A volume of 1 mL of overnight culture was used to inoculate 50 mL of Luria-Bertani medium. Culture was grown at 37°C and 225 rpm. Growth was monitored at A_{600} every 30 min. The doubling time was determined from the linear portion of the growth curve using the following equation:

$$\text{Doubling time} = \frac{\Delta\text{Time} \times \log 2}{\log(\text{Final conc.}) - \log(\text{Initial conc.})}.$$

Synthetic Methods

The ^{1}H and ^{13}C nuclear magnetic resonance (NMR) spectra were recorded on Bruker instruments at 400 MHz. Chemical shifts are reported in ppm and are referenced to residual DMSO solvent; 2.50 and 39.51 ppm for ^{1}H and ^{13}C, respectively. The high-resolution mass spectrometry was provided by the University of Connecticut Mass Spectrometry Laboratory using an AccuTOF mass spectrometer with a direct analysis in real time (DART) source. Optical rotation was measured on a Jasco P-2000 polarimeter at 589 nm. Thin-layer chromatography (TLC) analyses were performed on silica gel HL TLC plates (Sorbent Technologies). All glassware was oven-dried and allowed to cool under an argon atmosphere. Anhydrous dichloromethane, ether, and tetrahydrofuran were used directly from Baker CYCLE-TAINERS. Anhydrous dimethylformamide was purchased from Acros and degassed by purging with argon. All reagents were used directly from commercial sources unless otherwise stated. A premixed heterogeneous mixture of CuI (10% by weight) in $Pd(PPh_3)_2Cl_2$-(Pd/Cu) was used for the Sonogashira coupling.

Procedure for the Synthesis of (S)-4-(6-(4-(2,4-diamino-6-ethylpyrimidin-5-yl)but-3-yn-2-yl)benzo[d][1,3]dioxol-4-yl) benzoic Acid

We added ethyl-iododiaminopyrimidine (0.57 mmol, 0.15 g, 1 eq), Pd/Cu (0.05 mmol, 0.03 g, 0.08 eq), and KOAc (5.7 mmol, 0.55 g, 10 eq) to a 20 mL screw cap vial with a stir bar. Argon-purged anhydrous dimethylformamide (DMF) (0.05 M, 11.3 mL) was added followed by alkyne (0.73 mmol, 0.25 g, 1.3 eq). The reaction mixture was stirred under argon for 15 min and degassed once using a freeze/pump/thaw method. The vial was sealed under argon, heated at 60°C, and the reaction monitored by TLC. At the end of the reaction, the dark reddish brown solution was concentrated and the product purified by flash column chromatography (for pre-absorption of crude mixture: SiO_2 in 10% by weight of cysteine, 1.5 g; NH_2 capped SiO_2, 1.5 g; 13 g SiO_2 for column; and 2% MeOH/CH_2Cl_2) to afford the coupled pyrimidine as a pale-brown solid (0.2 g, 72% yield); TLC R_f = 0.4 (5% MeOH/CH_2Cl_2). The pyrimidine-coupled t-butyl ester product (0.0411 mmol, 0.02 g, 1 eq) in *d*-$CHCl_3$ (0.02 M, 2 mL) cooled to 0°C was deprotected using trifluoroacetic acid

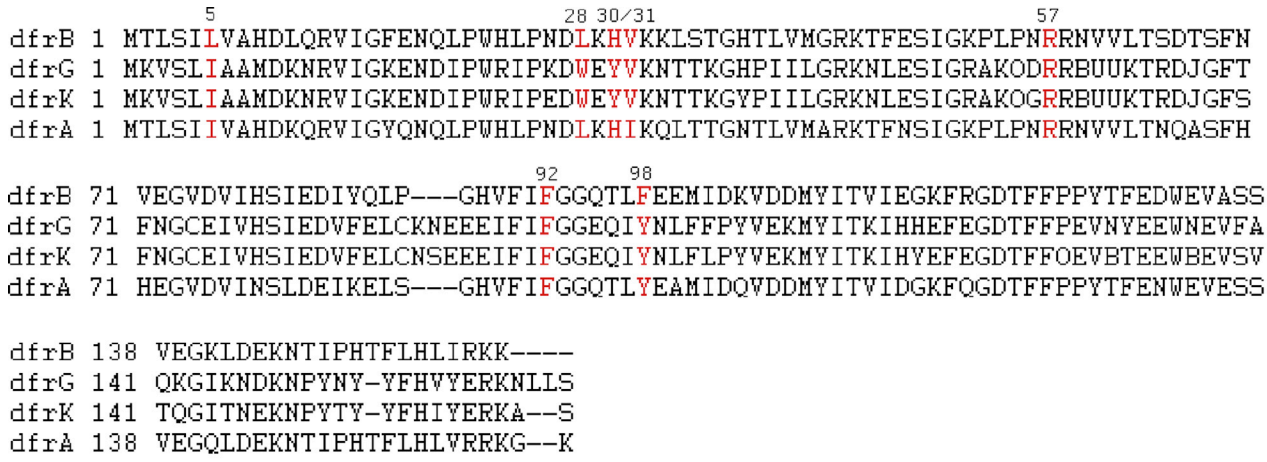

Figure 4. Sequence Alignment of Proteins Resulting from Chromosomal DHFR, *dfrB*, and Plasmid-Acquired DHFR Genes, *dfrG*, *dfrK*, and *dfrA*

(TFA) (8.22 mmol, 200 eq, 0.63 mL). After dropwise addition, the reaction mixture was brought to room temperature. At the end of the reaction, monitored by NMR, the reaction mixture was rotoevaporated at 20°C, and kept under vacuum for 15 min to remove excess TFA. Anhydrous CH_2Cl_2 was added to the product mixture containing a small amount of TFA for pre-absorption onto silica gel (1 g). Flash column chromatography was performed (5 g silica gel) initially with 100% EtOAc followed by 0.01% TFA in EtOAc; TLC R_f = 0.3 (10% MeOH/CH_2Cl_2 with 0.01% TFA). The clean fractions were rotoevaporated at 20°C ensuring complete removal of solvent. The oily TFA salt was neutralized with phosphate buffer at pH 7. The resulting white precipitate along with buffer solution was transferred to an Eppendorf tube and centrifuged to separate the water from the precipitate. After decanting the water layer, the white precipitate was rinsed with diethyl ether and methanol to remove the water. The dried white solids with a tinge of pink color (0.01 g, 57% yield) were subjected to characterization and biological evaluation. NMR spectra are shown in Figure S3. ^{1}H NMR (400 MHz, DMSO-*d*) δ 8.03 (d, *J* = 8.4 Hz, 2H), 7.86 (d, *J* = 8.4 Hz, 2H), 7.28 (s, 1H), 7.09 (s, 1H),6.28 (broad, 2H), 6.18 (s, 2H), 6.12 (s, 2H), 4.12 (q, *J* = 7 Hz, 1H), 2.55 (q, *J* = 7.6 Hz, 2H), 1.54 (d, *J* = 7.1 Hz, 3H), 1.11 (t, *J* = 7.6 Hz, 3H); ^{13}C NMR (100 MHz, DMSO-*d*) δ171.5, 167.1, 164.2, 161.1, 148.1, 143.4, 139.5, 138.4, 129.8, 129.7, 127.5, 120.2, 118.8, 107.3, 101.2, 100.5, 87.8, 76.0, 32.0, 28.8, 24.6, 12.4; and high-resolution mass spectrometry (HRMS) (DART, M^+ + H) *m/z* 431.1708 (calculated for $C_{24}H_{23}N_4O_4$, 431.1719); $[\alpha]^{24}$ + 3.3° (*c*, 0.146, DMSO).

(R)-4-(6-(4-(2,4-diamino-6-ethylpyrimidin-5-yl)but-3-yn-2-yl)benzo [d][1,3]dioxol-4-yl)benzoic Acid

We added ethyl-iododiaminopyrimidine (0.45 mmol, 0.12 g, 1 eq), Pd/Cu (0.04 mmol, 0.025 g, 0.08 eq), and KOAc (4.47 mmol, 0.44 g, 10 eq) to a 20 mL screw cap vial with a stir bar. Argon-purged anhydrous DMF (0.05 M, 8.9 mL) was added followed by alkyne (0.58 mmol, 0.20 g, 1.3 eq). Following the same workup as the (S) enantiomer, (R) enantiomer was obtained as a pale-brown solid (0.16 4 g, 75% yield); TLC R_f = 0.4 (5% MeOH/CH_2Cl_2). The pyrimidine-coupled t-butyl ester product (0.062 mmol, 0.03 g, 1 eq) in *d*-$CHCl_3$ (0.02 M, 3 mL) cooled to 0°C was deprotected using TFA (18.50 mmol, 300 eq, 1.42 mL). Repeating the same deprotection workup as above, (R) carboxylic acid was obtained as a white solid with a tinge of pink color (0.015 g, 56% yield); TLC R_f = 0.3 (10% MeOH/CH_2Cl_2 with 0.01% TFA). NMR spectra are shown in Figure S4. ^{1}H NMR (400 MHz, DMSO-*d*) δ 8.03 (d, *J* = 7.6 Hz, 2H), 7.87 (d, *J* = 7.2 Hz, 2H), 7.27 (s, 1H), 7.09 (s, 1H),6.26 (broad, 2H), 6.15 (s, 2H), 6.12 (s, 2H), 4.11 (q, *J* = 7 Hz, 1H), 2.56 (m, 2H), 1.53 (d, *J* = 7.0 Hz, 3H), 1.11 (t, *J* = 7.5 Hz, 3H); ^{13}C NMR (100 MHz, DMSO-*d*) δ171.6, 167.0, 164.2, 161.1, 148.1, 143.4, 139.5, 138.4, 129.8, 129.7, 127.5, 120.2, 118.8, 107.3, 101.2, 100.5, 87.8, 76.0, 32.0, 28.8, 24.6, 12.4; and HRMS (DART, M^+ + H) *m/z* 431.1708 (calculated for $C_{24}H_{23}N_4O_4$, 431.1719); $[\alpha]^{24}$ -5.2° (*c*, 0.143, DMSO).

SUPPLEMENTAL INFORMATION

Supplemental Information includes four figures and six tables and can be found with this article online at http://dx.doi.org/10.1016/j.chembiol.2016.11.007.

AUTHOR CONTRIBUTIONS

S.M.R. evaluated biological activity, characterized the strains, analyzed the genomes, and determined the crystal structure; E.W.S. synthesized compound UCP1175; S.K. synthesized compounds UCP1164, UCP1172, and UCP1173; N.D. synthesized compounds UCP1039, UCP1191, UCP1205, and UCP1206; J.K. expressed and purified DfrG; B.H. expressed and purified DfrA; J.F. assisted in enzymatic assays; M.N. provided strains from Hartford Hospital and consulted on clinical impact; J.A. provided strains from UConn Health and consulted on clinical impact, strain typing, and susceptibility analysis; D.L.W. directed all synthetic studies; A.C.A. directed all biological and structural studies. S.M.R., D.L.W., and A.C.A. wrote and edited the manuscript.

ACKNOWLEDGMENTS

We thank Lidia Beka and Dr. Joerg Graf for assistance in assembling the genomes and the UCONN MARS facilities, specifically Kendra Maas, for assistance with sequencing. We also acknowledge NIH grants AI104841 and AI 111957. D.L.W. declares that Spero Therapeutics licenses the development of the propargyl-linked antifolates from the University of Connecticut. D.L.W. serves as a consultant to Spero Therapeutics.

Received: June 11, 2016
Revised: September 15, 2016
Accepted: November 14, 2016
Published: December 8, 2016

REFERENCES

Adams, P.D., Afonine, P.V., Bunkóczi, G., Chen, V.B., Davis, I.W., Echols, N., Headd, J.J., Hung, L.-W., Kapral, G.J., Grosse-Kunstleve, R.W., et al. (2010). PHENIX: a comprehensive Python-based system for macromolecular structure solution. Acta Crystallogr. D Biol. Crystallogr. *66*, 213–221.

Aeschlimann, J.R., Dresser, L.D., Kaatz, G.W., and Rybak, M.J. (1999). Effects of NorA inhibitors on in vitro antibacterial activities and postantibiotic effects of levofloxacin, cirpofloxacin and norfloxacin in genetically related strains of *Staphylococcus aureus*. Antimicrob. Agents Chemother. *43*, 225–340.

Aziz, R.K., Bartels, D., Best, A.A., DeJongh, M., Disz, T., Edwards, R.A., Formsma, K., Gerdes, S., Glass, E.M., Kubal, M., et al. (2008). The RAST Server: rapid annotations using subsystems technology. BMC Genomics *9*, 75.

Bergmann, R., Van Der Linden, M., Chhatwal, G.S., and Nitsche-Schmitz, D.P. (2014). Factors that cause trimethoprim resistance in *Streptococcus pyogenes*. Antimicrob. Agents Chemother. *58*, 2281–2288.

Brettin, T., Davis, J.J., Disz, T., Edwards, R.A., Gerdes, S., Olsen, G.J., Olson, R., Overbeek, R., Parrello, B., Pusch, G.D., et al. (2015). RASTtk: a modular and extensible implementation of the RAST algorithm for building custom annotation pipelines and annotating batches of genomes. Sci. Rep. *5*, 1–6.

Bush, K., Leal, J., Fathima, S., Li, V., Vickers, D., Chui, L., Louie, M., Taylor, G., and Henderson, E. (2015). The molecular epidemiology of incident methicillin-resistant *Staphylococcus aureus* cases among hospitalized patients in Alberta, Canada: a retrospective cohort study. Antimicrob. Resist. Infect. Control *4*, 35.

Centers for Disease Control and Prevention. (2013). Centers for Disease Control and Prevention Outpatient Antibiotic Prescriptions — United States (CDC).

Clinical and Laboratory Standards Institute. (2014). CLSI Performance Standard for Antimicrobial Susceptibility Testing: Twenty-Fourth Informational Supplement (M100-S24) (CLSI).

Daigle, D.M., Hughes, D.W., and Wright, A.C. (1999). Prodigious substrate specificity of AAC(6')-APH(2″), an aminoglycoside antibiotic resistance determinant in enterococci and staphylococci. Chem. Biol. *6*, 99–110.

Dale, G.E., Broger, C., Hartman, P.G., Langen, H., Page, M.G.P., Then, R.L., and Stuber, D. (1995). Characterization of the gene for the chromosomal dihydrofolate reductase (DHFR) of *Staphylococcus epidermidis* ATCC 14990: the origin of the trimethoprim-resistant S1 DHFR from *Staphylococcus aureus*. J. Bacteriol. *177*, 2965–2970.

Dale, G.E., Broger, C., D'Arcy, A., Hartman, P.G., DeHoogt, R., Jolidon, S., Kompis, I., Labhardt, A.M., Langen, H., Locher, H., et al. (1997). A single amino acid substitution in *Staphylococcus aureus* dihydrofolate reductase determines trimethoprim resistance. J. Mol. Biol. *266*, 23–30.

Dao, B.D., Barreto, J.N., Wolf, R.C., Dierkhising, R.A., Plevak, M.F., and Tosh, P.K. (2014). Serum peak sulfamethoxazole concentrations demonstrate difficulty in achieving a target range: a retrospective cohort study. Curr. Ther. Res. Clin. Exp. *76*, 104–109.

de Gopegui, E.R., Juan, C., Zamorano, L., Pérez, J.L., and Oliver, A. (2012). Transferable multidrug resistance plasmid carrying cfr associated with tet (L), ant (4)-Ia, and dfrK genes from a clinical methicillin-resistant *Staphylococcus aureus* ST125 strain. Antimicrob. Agents Chemother. *56*, 2139–2142.

Emsley, P., and Cowtan, K. (2004). Coot: model-building tools for molecular graphics. Acta Crystallogr. D Biol. Crystallogr. *60*, 2126–2132.

Frei, C.R., Miller, M.L., Lewis, J.S., Lawson, K.A., Hunter, J.M., Oramasionwu, C.U., and Talbert, R.L. (2010). Trimethoprim-sulfamethoxazole or clindamycin for community-associated MRSA (CA-MRSA) skin infections. J. Am. Board Fam. Med. *23*, 714–719.

Frey, K.M., Liu, J., Lombardo, M.N., Bolstad, D.B., Wright, D.L., and Anderson, A.C. (2009). Crystal structures of wild-type and mutant methicillin-resistant *Staphylococcus aureus* dihydrofolate reductase reveal an alternate conformation of NADPH that may be linked to trimethoprim resistance. J. Mol. Biol. *387*, 1298–1308.

Frey, K.M., Lombardo, M.N., Wright, D.L., and Anderson, A.C. (2010a). Towards the understanding of resistance mechanisms in clinically isolated trimethoprim-resistant, methicillin-resistant *Staphylococcus aureus* dihydrofolate reductase. J. Struct. Biol. *170*, 93–97.

Frey, K.M., Georgiev, I., Donald, B.R., and Anderson, A.C. (2010b). Predicting resistance mutations using protein design algorithms. Proc. Natl. Acad. Sci. USA *107*, 13707–13712.

Frey, K.M., Viswanathan, K., Wright, D.L., and Anderson, A.C. (2012). Prospective screening of novel antibacterial inhibitors of dihydrofolate reductase for mutational resistance. Antimicrob. Agents Chemother. *56*, 3556–3562.

Gorwitz, R.J., Jernigan, D.B., Powers, J.H., and Jernigan, J.A. (2006). Participants in the CDC-convened Experts' Meeting on Management of MRSA in the Community: Summary of an Experts Meeting Convened by the Centers for Disease Control and Prevention. http://www.cdc.gov/mrsa/pdf/MRSA-Strategies-ExpMtgSummary-2006.pdf.

Hampele, I.C., D'Arcy, A., Dale, G.E., Kostrewa, D., Nielsen, J., Oefner, C., Page, M.G., Schönfeld, H.J., Stüber, D., and Then, R.L. (1997). Structure and function of the dihydropteroate synthase from *Staphylococcus aureus*. J. Mol. Biol. *268*, 21–30.

Heaslet, H., Harris, M., Fahnoe, K., Sarver, R., Putz, H., Chang, J., Subramanyam, C., Barreiro, G., and Miller, J.R. (2009). Structural comparison of chromosomal and exogenous dihydrofolate reductase from *Staphylococcus aureus* in complex with the potent inhibitor trimethoprim. Proteins *76*, 706–717.

Huovinen, P., Sundström, L., Swedberg, G., and Sköld, O. (1995). Trimethoprim and sulfonamide resistance. Antimicrob. Agents Chemother. *39*, 279.

Juda, M., Chudzik-Rzad, B., and Malm, A. (2016). The prevalence of genotypes that determine resistance to macrolides, lincosamides, and streptogramins B compared with spiramycin susceptibility among erythromycin-resistant *Staphylococcus epidermidis*. Mem. Inst. Oswaldo Cruz *111*, 155–160.

Kaatz, G.W., and Seo, S.M. (1995). Inducible NorA-mediated multidrug resistance in *Staphylococcus aureus*. Antimicrob. Agents Chemother. *39*, 2650–2655.

Kadlec, K., and Schwarz, S. (2010). Identification of a plasmid-borne resistance gene cluster comprising the resistance genes erm(T), dfrK, and tet(L) in a porcine methicillin-resistant *Staphylococcus aureus* ST398 strain. Antimicrob. Agents Chemother. *54*, 915–918.

Keshipeddy, S., Reeve, S.M., Anderson, A.C., and Wright, D.L. (2015). Non-racemic antifolates stereo-selectively recruit alternate cofactors and overcome resistance in *S. aureus*. J. Am. Chem. Soc. *137*, 8983–8990.

Khan, S.A., Nawasz, M.S., Khan, A.A., and Cerniglia, C.E. (1999). Simultaneous detection of erythromycin-resistant methylase genes ermA and ermC from *Staphylococcus* spp. by multiplex-PCR. Mol. Cell. Probes *13*, 381–387.

Lamb, K.M., Lombardo, M.N., Alverson, J., Priestley, N.D., Wright, D.L., and Anderson, A.C. (2014). Crystal structures of *Klebsiella pneumoniae* dihydrofolate reductase bound to propargyl-linked antifolates reveal features for potency and selectivity. Antimicrob. Agents Chemother. *58*, 7484–7491.

Li, L., Feng, W., Zhang, Z., Xue, H., and Zhao, X. (2015). Macolide-lincosamide-streptogramin resistance phenotypes and genotypes of coagulase-positive *Staphylococcus aureus* and coagulase-negative staphylococcal isolates from bovine mastitis. BMC Vet. Res. *11*, 1–8.

Lina, G., Piemont, Y., Godail-Gomot, F., Bes, M., Peter, M., Gauduchon, V., Vandenesch, F., and Etienne, J. (1999). Panton-Valentine leukocidin in staphylococcal infections. Clin. Infect. Dis. *29*, 1128–1132.

Liu, C., Bayer, A., Cosgrove, S.E., Daum, R.S., Fridkin, S.K., Gorwitz, R.J., Kaplan, S.L., Karchmer, A.W., Levine, D.P., Murray, B.E., et al. (2011). Clinical practice guidelines by the Infectious Diseases Society of America for the treatment of methicillin-resistant *Staphylococcus aureus* infections in adults and children. Clin. Infect. Dis. *52*, 18–55.

Lodise, T.P., Jr., and McKinnon, P.S. (2007). Burden of methicillin-resistant *Staphylococcus aureus*: focus on clinical and economic outcomes. Pharmacotherapy *27*, 1001–1012.

Lombardo, M.N., G-Dayanandan, N., Wright, D.L., and Anderson, A.C. (2016). Crystal structures of trimethoprim-resistant DfrA1 rationalize potent Inhibition by propargyl-linked antifolates. ACS Infect. Dis. *2*, 149–156.

Matsuoka, M., Inoue, M., Endo, Y., and Nakajima, Y. (2003). Characterization and expression of three genes, msr(A), mph(C) and erm(Y), that confer resistance to macrolide antibiotics in *Staphylococcus aureus*. FEMS Micro. Lett. *220*, 287–293.

Nathwani, D., Morgan, M., Masterton, R.G., Dryden, M., Cookson, B.D., French, G., and Lewis, D. (2008). Guidelines for UK practice for the diagnosis and management of methicillin-resistant *Staphylococcus aureus* (MRSA) infections presenting in the community. J. Antimicrob. Chemother. *61*, 976–994.

Nurjadi, D., Olalekan, A.O., Layer, F., Shittu, A.O., Alabi, A., Ghebremedhin, B., Schaumburg, F., Hofmann-Eifler, J., Van Genderen, P.J.J., Caumes, E., et al. (2014). Emergence of trimethoprim resistance gene dfrG in *Staphylococcus aureus* causing human infection and colonization in sub-Saharan Africa and its import to Europe. J. Antimicrob. Chemother. *69*, 2361–2368.

Nurjadi, D., Friedrich-Jänicke, B., Schäfer, J., Van Genderen, P.J.J., Goorhuis, A., Perignon, A., Neumayr, A., Mueller, A., Kantele, A., Schunk, M., et al. (2015). Skin and soft tissue infections in intercontinental travellers and the import of multi-resistant *Staphylococcus aureus* to Europe. Clin. Microbiol. Infect. *21*, 567.

Oefner, C., Parisi, S., Schulz, H., Lociuro, S., and Dale, G.E. (2009a). Inhibitory properties and X-ray crystallographic study of the binding of AR-101, AR-102 and iclaprim in ternary complexes with NADPH and dihydrofolate reductase from *Staphylococcus aureus*. Acta Crystallogr. D Biol. Crystallogr. *65*, 751–757.

Oefner, C., Bandera, M., Haldimann, A., Laue, H., Schulz, H., Mukhija, S., Parisi, S., Weiss, L., Lociuro, S., and Dale, G.E. (2009b). Increased hydrophobic interactions of iclaprim with *Staphylococcus aureus* dihydrofolate reductase are responsible for the increase in affinity and antibacterial activity. J. Antimicrob. Chemother. *63*, 687–698.

Overbeek, R., Olson, R., Pusch, G.D., Olsen, G.J., Davis, J.J., Disz, T., Edwards, R.A., Gerdes, S., Parrello, B., Shukla, M., et al. (2014). The SEED and the rapid annotation of microbial genomes using subsystems technology (RAST). Nucleic Acids Res. *42*, D206–D214.

Pan, X., Hamlyn, P.J., Talens-Visconti, R., Alovero, F.L., Manzo, R.H., and Fisher, L.M. (2002). Small-colony mutants of *Staphylococcus aureus* allow selection of gyrase-mediated resistance to dual-target fluoroquinolones. Antimicrob. Agents Chemother. *46*, 2498–2506.

Pate, A.J., Terribilini, R.G., Ghobadi, F., Azhir, A., Barber, A., Pearson, J.M., Kalantari, H., and Hassen, G.W. (2014). Antibiotics for methicillin-resistant *Staphylococcus aureus* skin and soft tissue infections: the challenge of outpatient therapy. Am. J. Emerg. Med. *32*, 135–138.

Petersson, A.C., Olsson-Liljequist, B., Miörner, H., and Haeggman, S. (2010). Evaluating the usefulness of spa typing, in comparison with pulsed-field gel electrophoresis, for epidemiological typing of methicillin-resistant *Staphylococcus aureus* in a low-prevalence region in Sweden 2000-2004. Clin. Microbiol. Infect. *16*, 456–462.

Reeve, S.M., Gainza, P., Frey, K.M., Georgiev, I., Donald, B.R., and Anderson, A.C. (2014). Protein design algorithms predict viable resistance to an experimental antifolate. Proc. Natl. Acad. Sci. USA *112*, 749–754.

Reeve, S.M., Scocchera, E.W., Ferriera, J.F., Dayanadan, N.G., Keshipeddy, S., Wright, D.L., and Anderson, A.C. (2016). Charged propargyn-linked antifolates reveal mechanisms of antifolate resistance and inhibit trimethoprim-resistant MRSA strains possessing clinically relevant mutations. J. Med. Chem. *59*, 6493–6500.

Sader, H.S., Farrell, D.J., Flamm, R.K., and Jones, R.N. (2015). Activity of ceftaroline and comparator agents tested against *Staphylococcus aureus* from patients with bloodstream infections in US medical centres (2009-13). J. Antimicrob. Chemother. *70*, 2053–2056.

Schmitz, F., Jones, M.E., Hofmann, B., Hansen, B., Scheuring, S., Luckefahr, M., Fluit, A., Verhoef, J., Hadding, U., Heinz, H., and Kohrer, K. (1998). Characterization of grlA, grlB, gyrA and gyrB mutations in 116 unrelated isolates of *Staphylococcus aureus* and effects of mutations on ciprofloxacin. Antimicrob. Agents Chemother. *42*, 1249–1252.

Scocchera, E., Reeve, S.M., Keshipeddy, S., Lombardo, M.N., Hajian, B., Sochia, A.E., Alverson, J.B., Priestley, N.D., Anderson, A.C., and Wright, D.L. (2016). Charged nonclassical antifolates with activity against Gram-positive and Gram-negative pathogens. ACS Med. Chem. Lett. *7*, 692–696.

Sekiguchi, J., Tharavichitkul, P., Miyoshi-Akiyama, T., Chupia, V., Fujino, T., Araake, M., Irie, A., Morita, K., Kuratsuji, T., and Kirikae, T. (2005). Cloning and characterization of a novel trimethoprim-resistant dihydrofolate reductase from a nosocomial isolate of *Staphylococcus aureus* CM. S2 (IMCJ1454). Antimicrob. Agents Chemother. *49*, 3948–3951.

Trzcinski, K., Cooper, B.S., Hryniewicz, W., and Dowson, C.G. (2000). Expression of resistance to tetracyclines in strains of methicillin-resistant *Staphylococcus aureus*. J. Antimicrob. Chemother. *45*, 763–770.

Cell Chemical Biology, Volume *23*

Supplemental Information

MRSA Isolates from United States Hospitals Carry *dfrG* and *dfrK* Resistance Genes and Succumb to Propargyl-Linked Antifolates

Stephanie M. Reeve, Eric W. Scocchera, Narendran G-Dayanadan, Santosh Keshipeddy, Jolanta Krucinska, Behnoush Hajian, Jacob Ferreira, Michael Nailor, Jeffrey Aeschlimann, Dennis L. Wright, and Amy C. Anderson

Table S1. Related to Table 1. Antibiotic Susceptibility Profiles of Clinical MRSA Isolates (μg/mL)

Strain	Erythromycin	Clindamycin	Tetracycline	Gentamicin	Levofloxacin	Ciprofloxacin	Gatifloxacin
UCH MRSA 1	>4 (R)	≤0.12 (S)	≤2 (S)	≤2 (S)	64 (R)	>64 (R)	>8(R)
UCH MRSA 115	<0.25 (S)	≤0.12 (S)	>16 (R)	>16 (R)	>64 (R)	>64 (R)	>8(R)
UCH MRSA 121	>4 (R)	0.25 (S)	≤2 (S)	≤2 (S)	>64 (R)	64 (R)	>8(R)
UCH MRSA 127	>4 (R)	≤0.12 (S)	≤2 (S)	≤2 (S)	8 (R)	32 (R)	4(R)
HH MRSA 714	2 (R)	≤0.12 (S)	≤2 (S)	≤2 (S)	>64 (R)	64 (R)	>8(R)
HH MRSA 1144	>4 (R)	>2 (R)	>16 (R)	>16 (R)	8 (R)	64 (R)	4 (R)
HH MRSA 1184	>4 (R)	0.25 (S)	≤2 (S)	≤2 (S)	0.25 (S)	1 (S)	<1 (S)
UCH MSSA 1	>4 (R)	>2 (R)	≤2 (S)	≤2 (S)	8 (R)	64 (R)	2 (S)

All strains are sensitive to synercid (MIC ≤0.5μg/mL), daptomycin (MIC ≤ 0.5 μg/mL), rifampin (MIC≤ 0.5μg/mL), vancomycin (MIC ≤2 μg/mL), streptomycin (MIC ≤1000 μg/mL), and linezolid (MIC ≤1 μg/mL). All strains are resistant to ampicillin (MIC≥16 μg/mL), penicillin (MIC >8 μg/mL). UCH MSSA-1 is sensitive to oxacillin.

Table S2. Related to Table 1 and Table S1. Molecular Mechanisms of Antibiotic Resistance for Clinical Isolates

	Resistance Mechanism	MIC Range (ug/mL)	Strains
Trimethoprim	*dfrA*	250	UCH115, HH1144
	dfrG	>1000	UCH MRSA1, UCH121, UCH127, HH714, UCH MSSA1
	dfrK	>1000	HH1184
Sulfamethoxazole	*folB*(F17L, V30I, T31N, M37I, I58V, T59S, V60L, L64M, I110M, V117I, V126I, E208K, F226L)	>500	UCH MRSA1
	folB(F17L, T28S, T59S, L64M, E205K)	≥500	UCH115, UCH 121, UCH127, HH714, HH1144, UCH MSSA1
	folB (V30I, I58V, T59S,V60L, L64M, I100M, V117I, V126I, F226L)	32	HH1184
Tetracycline	*TetM*	>16	UCH115, HH1144
Gentamicin	aac(2')-apc(6")	>16	UCH115, HH1144
Erythromycin	*mphC*	8-32	UCH121, UCH127, HH1184
	ermC	>64	UCH MRSA1, HH1144, UCH MSSA 1
Clindamycin	*ermC*	>64	UCH MRSA1, HH1144, UCH MSSA 1
Levofloxacin/ Ciproflxacin/ Gatifloxacin	*gryA*(S84R ,S85P), *grlA*(S80F), *grlB*(E471K)	64/ >64/>8	UCH MRSA1
	gryA(S84L, S85P), gyrA(S90K, E84K)	>64/>64/ >8	UCH115
	gryA(S84R ,S85P), *grlA*(S80F), *grlB*(D432V)	>64/64/>8	UCH121, HH714
	gyrA (S84L) and *grlA* (S80F), *grlB*(D432V, E596D*)	8/32/4	UCH127
	gyrA (S84L) and *grlA* (S80F)	8/64/4	HH1144
Levofloxacin/ Ciproflxacin	*gyrA*(S84L)	8/64	UCH MSSA1

Table S3. Related to Table 2. Fluoroquinolone Minimum Inhibitory Concentrations Supplemented with Reserpine (μg/mL)

	Minimum Inhibitory Concentration		Minimum Inhibitory Concentration with 20 ug/mL Reserpine	
Strain	**Levofloxacin**	**Ciprofloxacin**	**Levofloxacin**	**Ciprofloxacin**
UCH MRSA 1	64	>64	64 (1)	32 (≥2)
UCH MRSA 115	>64	>64	>64 (≥1)	32 (≥2)
UCH MRSA 121	>64	64	>64 (≥1)	32 (2)
UCH MRSA 127	8	32	4 (2)	8 (4)
HH MRSA 714	>64	64	>64 (≥1)	32 (2)
HH MRSA 1144	8	64	8 (1)	16 (4)
HH MRSA 1184	0.25	1	<0.125 (≥2)	<0.125 (>4)
UCH MSSA 1	8	64	8 (1)	32 (2)

Fold increases in MIC noted in parenthases

Table S4. Related to Table 2. Synergy Minimum Inhibitory Concentrations Supplemented with Sulfamethoxazole (μg/mL)

Strain		**UCP1039**	**UCP1164**	**UCP1172**	**UCP1173**	**UCP1191**	**UCP1205**	**UCP1206**
UCHC MRSA 115	*dfrA*	1.25	0.3125	1.25	0.1563	0.625	2.5	0.625
HH MRSA 714	*dfrG*	0.0391	0.3125	0.3125	0.3125	0.0391	0.0391	0.1563
HH MRSA 1184	*dfrK*	≤0.0098	≤0.0098	≤0.0098	≤0.0098	≤0.0098	≤0.0098	≤0.0098

*UCH MRSA115 and HH MRSA115 contained 100 μg/mL SMX and HH MRSA1184 contains 10 μg/mL

Table S5. Related to Figure 2. Crystallography Data Collection and Structure Refinement Statistics

	DfrB :NADPH:UCP1191
PDB ID	5JG0
Space group	$P6_122$
No. monomers in asymmetric unit	1
Unit cell (*a, b, c* in Å)	78.86, 78.86, 106.43 90.0, 90.0, 120.0
Resolution (Å)	39.44-1.88 (1.91-1.88)
Completeness % (last shell, %)	99.75 (97.0)
Unique reflections	16, 498
Redundancy (last shell)	16.7 (17.4)
Rsym, (last shell)	0.107 (0.483)
$<I/\sigma>$ (last shell)	41.2 (5.52)
R-factor/Rfree	0.1765/ 0.2172
No. of atoms (protein, ligands, solvent)	1,458
Rms deviation bond lengths (Å), angles (deg)	0.007, 1.238
Average B factor for protein ($Å^2$)	29.54
Average B factor for ligand ($Å^2$)	25.34 β-NADPH 34.66 Inhibitor
Average B factor for solvent molecules ($Å^2$)	35.74
Residues in most favored regions (%)[a]	98.12
Residues in additional allowed regions (%)[a]	1.88
Residues in disallowed regions (%)[a]	0
Collection Location	SSRL Beamline 7-1

[a] According to an analysis of the Ramachandran plot

Table S6. Related to Figure 3. Structural analysis of residues involved in binding PLAs and NADPH

DfrB:PLA Interactions			
Residue	**Binding Partner**	**Bond Distance (Å)**	**Comments**
Leu5	Backbone to C_2-NH_3	2.9	Leu5Ile Mutation in all TMP^R enzymes
Asp27	Side chain to C_4-NH_3,	3.2	Conserved in all *dfr* enzymes
	Side chain to N_5	2.6	
Leu28	Hydrophobic interactions with B-C ring system and C_6 ethyl		Leu28Tyr mutation in *dfrG/K* no mutation in *dfrA*
His30	Coordinates H_2O with pyrimidine C_4-NH_3	3.1, 3.2	His30Tyr mutations in *dfrK/G,* mutations known to be relevant[1]
Val31	Hydrophobic interaction with pyrimidine C_6-ethyl		Val31Ile in *dfrA*, mutations known to be relevant[2]
Ile50	Side chains make hydrophobic interactions with B-C ring system		Conserved in all *dfr* enzymes
Leu54			Conserved in all *dfr* enzymes
Arg57	Side chain to C-ring COOH	2.8	Conserved in all *dfr* enzymes
Phe92	Backbone to pyrimidine C_2-NH_3	3.1	Conserved in all *dfr* enzymes
Phe98	Mutations known to be relevant[3]		Phe98Tyr mutation in all *dfr* enzymes.
DfrB:NADPH Interactions			
Residue	**Binding Partners**	**Bond Distances (Å)**	**Comments**
Ala7	BB Carbonyl to Nicotinamide amide (NH_2)	2.8	Conserved in all *dfr* enzymes
	BB amine to Nicotinamide amide (OH)	2.7	
Gln19	Nicotinamide ribose	3.3	Gln19Asp in *dfrG/K*
Arg44	Guanidine to ribose phosphate	3.2	Conserved in all *dfr* enzymes
	γ –NH to ribose phosphate	2.9	
Thr46	Side chain to phosphate	2.5	Thr46His in *dfrG/K*
Thr63	Side chain to ribose phosphate	2.8	Conserved in all *dfr* enzymes
Glu100	Side chain to adenine	2.9/2.7	Glu100Leu in *dfrG/K* Glu100Ala in *dfrA*

(BB) Backbone (SC) side chain

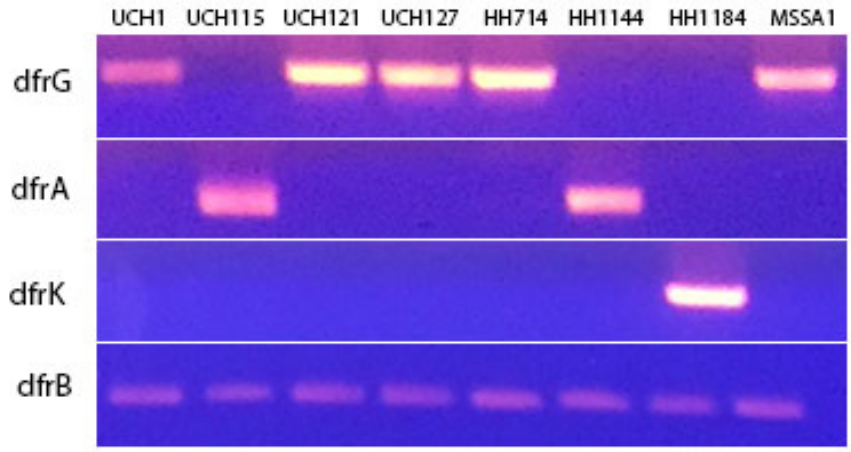

Figure S1. Related to Table 1. Composite PCR Gel for Gene Identification

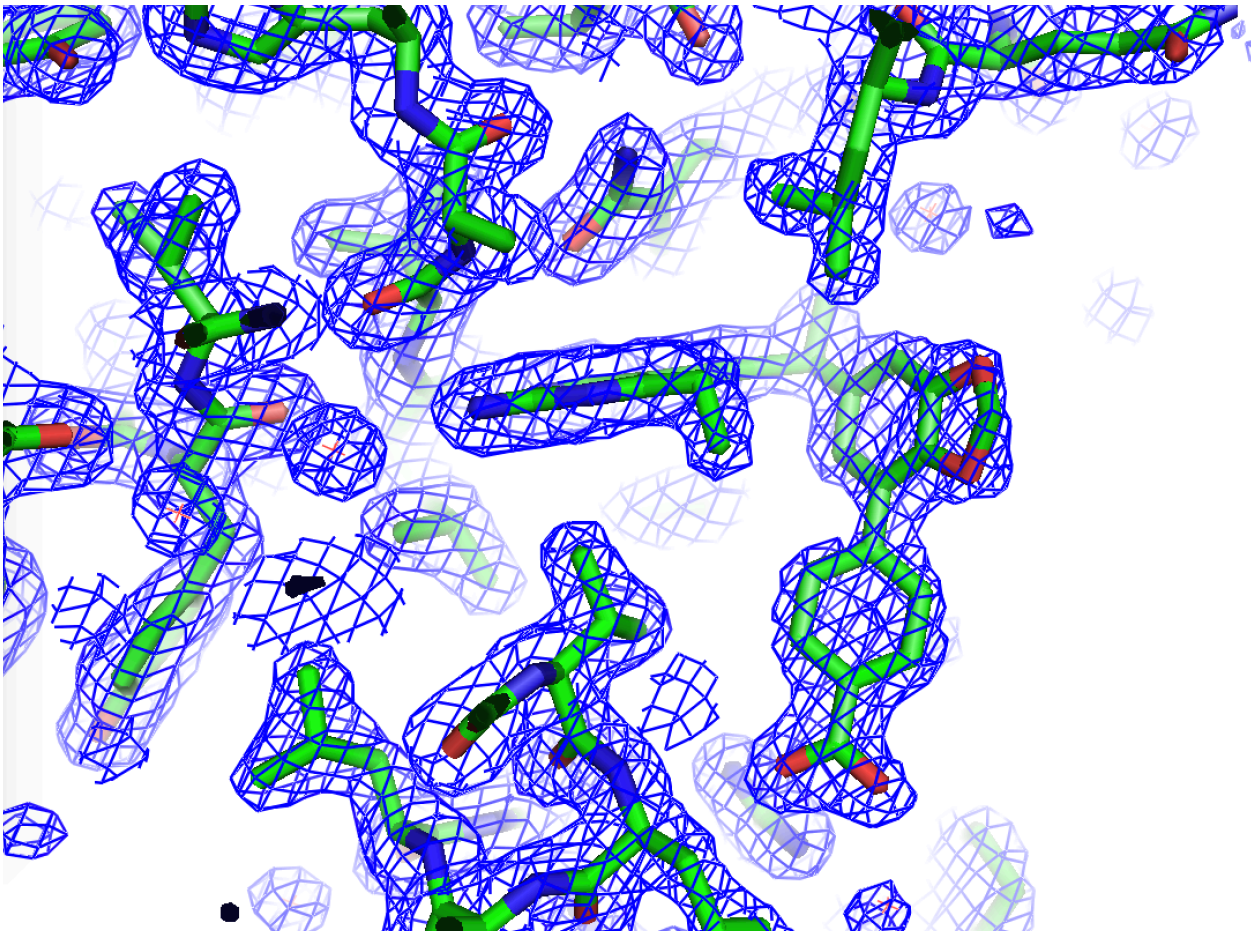

Figure S2. Related to Figure 2. OMIT Map from crystal structure of SaDHFR bound to NADPH and UCP1191.

Electron density (2Fo-Fc) of the active site residues for the Sa(WT)DHFR:NADPH:UCP1191, shown at 1.0σ

Fig. S3. Related to Experimetnal. ^{1}H and ^{13}C NMR of UCP1205

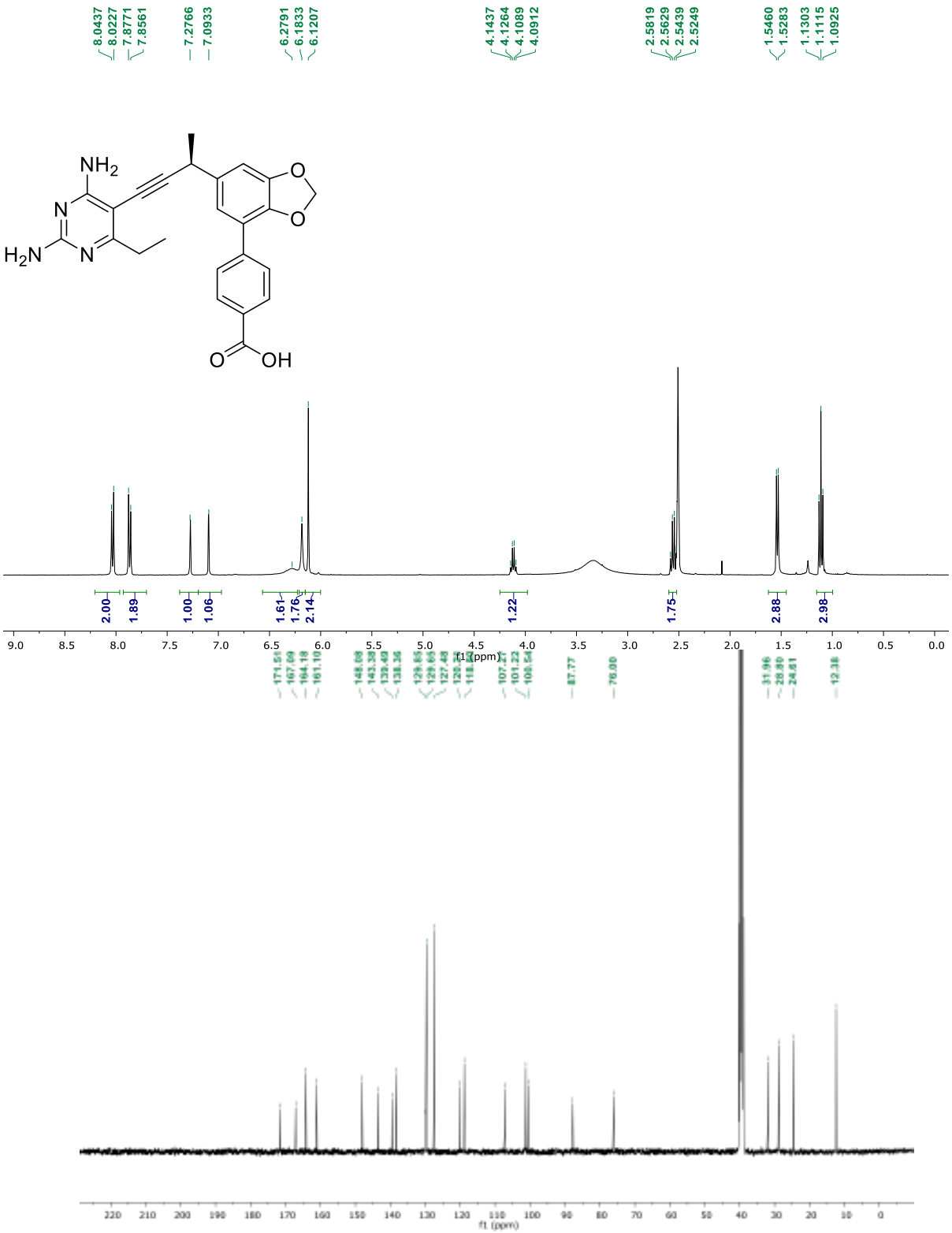

Fig. S4. Related to Experimental. ^{1}H and ^{13C}NMR of UCP1206